Spatial multi-omics reveals a cancer-associated fibroblast-T cell niche sustaining tissue-resident immunity in clear-cell renal cell carcinoma

Zhenghui Hu, Feifan Wang, Yiwei Lin

Department of Urology, The First Affiliated Hospital, Zhejiang University School of Medicine, Hangzhou, China

Contributions: (I) Conception and design: Z Hu; (II) Administrative support: Y Lin; (III) Provision of study materials or patients: None; (IV) Collection and assembly of data: Z Hu, F Wang; (V) Data analysis and interpretation: Z Hu, F Wang; (VI) Manuscript writing: All authors; (VII) Final approval of manuscript: All authors.

Correspondence to: Yiwei Lin, PhD. Department of Urology, The First Affiliated Hospital, Zhejiang University School of Medicine, 79 Qingchun Road, Shangcheng District, Hangzhou 310003, China. Email: zjulyw@zju.edu.cn.

Background: Clear-cell renal cell carcinoma (ccRCC) has a lot of immune cells in it, but the performance of the body's immune system against ccRCC and the outcome for patients who have ccRCC vary greatly. Recent studies indicate that not only how many immune cells are present, but also the state of those cells and how they are arranged within the tumor microenvironment (TME) contribute to how well an individual's immune system can eliminate ccRCC. Therefore, this study aimed to systematically characterize the spatial organization and functional interactions of immune and stromal cells in ccRCC using integrated single-cell and spatial multi-omics approaches.

Methods: To better understand ccRCC through this multi-omics analysis, we utilized two cohort studies of single-cell RNA sequencing (scRNA-seq) data combined with spatial transcriptomics (sRNA-seq) data to make a multi-omics atlas of ccRCC. We performed in-depth functional enrichment analysis, survival analysis, modeling of cell-to-cell communication, as well as spatial validation of these analyses, to identify the heterogeneous nature of cell-cell interactions *in vivo* within the ccRCC TME and determine how they correlate and contribute to prognostic outcomes for ccRCC patients.

Results: We identified various epithelial, immune, and mesenchymal cell states in ccRCC, showing distinct differences in their prognostic values: CD4 Trm, iCAFs, PDGFRB^{+} mesenchymal cells, and proximal tubule-like epithelial programs had positive prognostic associations, while resident CD8 T cells and ascending thin limb-like epithelial cell programs had negative prognostic associations. Spatial and computational analyses of these results showed the presence of a secure iCAF-CD4 Trm cell niche, with fibronectin-integrin α5β1 signaling as an anchor for CD4 Trm residency, located at the tumor-stroma interface.

Conclusions: These results demonstrate that the prognosis of ccRCC is determined by the spatial organization of the immune-stromal cell niche rather than just by the number of immune cells present. The iCAF-CD4 Trm axes may provide opportunities for precision immunomodulatory therapy.

Keywords: Clear-cell renal cell carcinoma (ccRCC); single-cell RNA sequencing (scRNA-seq); spatial transcriptomics; tumor microenvironment (TME); cancer-associated fibroblasts (CAFs)

Submitted Jan 07, 2026. Accepted for publication Mar 05, 2026. Published online Mar 26, 2026.
doi: 10.21037/tau-2026-1-0017
View this article at: https://dx.doi.org/10.21037/tau-2026-1-0017

Introduction

Clear-cell renal cell carcinoma (ccRCC) has an immune suppressed tumor microenvironment (TME), which allows the tumor to continue growing, resistant to therapies (1). Cancer-associated fibroblasts (CAFs), which are prevalent in ccRCC, alter the TME through extracellular matrix (ECM) remodeling and altering the function of immune cells (2). CAFs stimulate a cycle of immune evasion by inducing M2 (TAM) like polarization of tumor-associated macrophages (TAMs) and the expansion of regulatory T cells (Tregs), forming a multi-tiered network of immunosuppression (3). ECM barriers formed by CAFs also reduce the influx of cytotoxic T lymphocytes (CTLs) leading to less T cell infiltration into tumor islets and exacerbating immune escape (3). All these contribute to ccRCC's well-known resistance to immunotherapy and targeted therapies. For example, ccRCC has a high fibroblast content and low levels of T cell infiltration, which correlates with worse responses to immune checkpoint blockade (4). Recent evidence from recurrent RCC indicates that CAFs can induce apoptosis of $CD8^+$ T cells by secreting galectin-1, therefore diminishing anti-tumor immunity (5). Thus, CAFs are clearly important regulators of the immune landscape in kidney cancer.

Even though CAFs are thought to be largely immunosuppressive, recent research indicates that various types of CAFs [e.g., myofibroblastic CAFs (MyCAFs) and inflammatory CAFs (iCAFs)] exist within the TME, and that these different receptors confer different properties. Two main CAF subtypes have been reported in solid tumors (6): MyCAFs, a source of fibrillar collagen; and iCAFs, used initially in pancreatic cancer. MyCAFs produce α-smooth muscle actin and use transforming growth factor beta (TGF-β) to drive the production of collagen-based substrates and coupling systems to provide a contractile, dense stroma that supports tumor development. In contrast, iCAFs generally secrete several inflammatory modulating factors [interleukin-6 (IL-6), leukaemia inhibitory factor (LIF), etc.] as well as chemokines CXCL-12 to promote a pro-inflammatory and anti-cytotoxic T-cell environment via direct secretion and via recruitment from other stroma. Moreover, although each CAF subtype can play a role in the suppression of tumor growth, some CAFs have the potential to develop major histocompatibility complex class II (MHC II) ability and interact with T cells. An example of this is with CAFs in the non-small cell lung cancer context, as some MHC II+ CAFs directly activate effector $CD4^+$ T cells, preventing their apoptosis through C1q-C1qbp signaling pathways (7). Moreover, CAFs with MHC II deficiency or C1q deficiency have been shown to accelerate tumor growth in non-small cell lung cancer tissues, indicating that certain CAFs can mediate an immunogenic effect (7). This suggests that the immunosuppressive functions of CAFs are not universal, their immunogenic factors will depend on a variety of different interactions with immune cells and the surrounding microenvironment.

T cells also show a variety of phenotypes in ccRCC. Most tumors present with an "immune exclusion" pattern, with many T cells being in the peritumoral stroma, rather than infiltrating into the nests of tumor cells. A significant percentage of the T cells within the peritumoral stromal compartment is be tissue-resident memory T cells (Trm), marked by biomarker expression (CD69, CD103) and an exhausted or pre-exhausted transcription profile. Trm cells have recently been documented as key components of the anti-tumor immune response in many cancers, with the presence of these cells often correlating with longer patient

Highlight box

Key findings

- Integrated single-cell and spatial transcriptomic analyses showed that there is significant diversity in the immune, stromal, and epithelium of clear cell renal cell carcinoma (ccRCC).
- The combined spatial and computational analyses highlight a well-defined iCAF-CD4 Trm area located at the tumor-stroma interface that is functionally supported by extracellular matrix-integrin signaling, with CD4 Trm residency being anchored by fibronectin-integrin α5β1.

What is known and what is new?

- The ccRCC has significant immune infiltrate; however immune abundance predicts neither clinical outcome nor immunotherapeutic response.
- This study demonstrates that ccRCC prognosis is determined by specific cellular states and spatially organized immune-stromal niches and identifies an iCAF-CD4 Trm axis as a key determinant of protective immunity.

What is the implication, and what should change now?

- The results of these studies point towards the need for a location-based (or niche) approach to support anti-tumor immune responses, as opposed to relying on broad distribution of immune cells throughout the body.
- Future therapeutic strategies should focus on preserving or reprogramming immune-supportive stromal states and reinforcing tissue-resident T-cell niches, potentially enhancing responses to immunotherapy and enabling more precise patient stratification.

survival and improved responses to immunotherapy (8). Trm cells also provide long-term local immune surveillance and can mount rapid effector responses upon subsequent encounters with antigen. Indeed, increased Trm infiltration correlates with positive clinical outcomes in melanoma, ovarian cancer, and other solid tumors (9-11). However, this population of T cells is heterogeneous; within ccRCC, researchers have documented that $CD8^+$ Trm can exist in an exhausted state limiting their cytotoxic potential in the short-term (12). Conversely, although $CD4^+$ tissue-resident T cells are less studied in RCC, these may provide "help" for orchestrating local immune responses or in maintaining the function of B cells and dendritic cells (DCs) in tertiary lymphoid structures. Therefore, the balance between $CD8^+$ T cell cytotoxicity, Trm subsets, and Tregs may be critical in determining whether the immune microenvironment is permissive for tumor eradication or immune evasion.

As noted in the previous paragraph, researchers should consider using appropriate spatial multi-omics technologies as they seek to understand how these distinct cell types interact with each other and impact patient outcome. Bulk analysis does not provide spatial context, whereas the information generated from the same genes expressed with single-cell RNA sequencing (scRNA-seq) only provides a snapshot of the cellular architecture at a single time point; there is no way to know where these cells are distributed within their environment. For this study, we combined single cell transcriptomic data with data on how gene expression varies with position to provide a more complete understanding of the architecture of ccRCC, as well as identifing relevant ligand-receptor interactions that influence the development and maintenance of immune niches. Using gene expression analysis, communication of cells based upon the expression of genes, and the spatial location of both types of cells, this study provided substantial evidence for the establishment of a novel CAF-T cell niche adjacent to the ccRCC tumor margin that supports the infiltration of tissue resident T cells. The presence of this niche was associated with a significantly improved prognosis. This study also pointed out that, as was pointed out by a number of recent research articles, the use of both sequencing technology in conjunction with spatially-based technology represents an important and immediate need to further understand the temporal and spatial heterogeneity associated with different CAF subtypes and immune cell types in order to develop precision-based approaches to therapeutic intervention.

Methods

Sample collection and datasets

The present work analyzed two published scRNA-seq datasets from human ccRCC and normal kidney tissue (GSE210042 and GSE156632), which included 26 samples of ccRCC and 7 samples of control (normal) kidneys (2,13). In addition, we reviewed a spatial transcriptomics dataset (10x Genomics Visium) that included the same tumor and normal tissue samples (GSE175540) (14). Clinical data associated with each sample included survival outcome and treatment-naïve patients. All clinical data are processed from the raw count data of each of these datasets. Survival analysis involved grouping patients based on high *vs.* low (above *vs.* below median) gene signature scores or by the proportion of their clusters. The study was conducted in accordance with the Declaration of Helsinki and its subsequent amendments.

scRNA-seq analysis

Scanning scRNA-seq data preprocessing performed through Seurat using R. Filtering performed for cells with >20% mitochondrial genes and <200 genes detected. Doublets are identified using the DoubletFinder algorithm. Cells exhibiting abnormal gene counts or elevated RNA content are subsequently removed. Data Normalization was achieved using SCTransform method, and integration of multiple datasets was performed using Seurat Anchors workflow (15). Utilization of principal component analysis (PCA) for the selection of statistically significant principal components (PCs). Clustering was performed using 0.4–0.8 resolution range based on biological relevance of the resultant clusters. Clusters annotated using known lineage markers. To determine differential expressions of genes (DEGs) within each cluster, Wilcoxon rank-sum test (using Seurat FindMarkers, with log_fc_threshold of 0.25 and P value under Bonferroni correction of 0.05) was used. Major immune compartments (T-cells, myeloid, and fibroblasts) are further subclustered to provide a clearer understanding of the diverse subtypes. To perform gene set enrichment analysis, Gene Ontology (GO) and Kyoto Encyclopedia of Genes and Genomes (KEGG) pathway analysis are completed for cluster-specific DEGs using clusterProfiler within R (16).

Spatial transcriptomics integration

Seurat's Spatial transcriptomics data (Visium) was assessed

using the spatial analysis (SPC) method. All spots are normalized and scaled as part of preprocessing steps. PCA was conducted on the top 2,000 variable genes followed by clustering (by setting a resolution of 0.5) to identify the spatial expression domains. As part of the integration of the single cell and spatial data the authors used Seurat's label transfer methodology with the scRNA-seq dataset as a reference. Find transfer anchors was applied using the default parameters (canonical correlation analysis with L2 Normalization) in order to correctly assign the cell types defined by the single cells to the Visium spots (15). This provided an estimate of the spatial distribution of the relative abundance of each cell type. The authors also averaged the top 20 marker genes to create a gene signature for each of the key clusters, which they then computed spot-wise using a map of the marker genes against the spots in the Visium sequencing sample, to determine if the presence of one type of cell is statistically associated with the presence of another type of cell. To assess the spatial colocalization of these gene signatures the authors calculated the Pearson correlation coefficient for the spatial gene expression patterns of each pair of cell types or gene signatures. It respects to where they are in the tissue and used a permutation test on the observed enrichment of adjacent spots. The authors defined locations where there was a high frequency of co-occurrence of iCAF and CD4 Trm cells (spatially co-located) as "mixed spots" within the CAF–Trm niche.

Cell-cell interaction analysis

Using CellChat on the scRNA-seq data, we analyses intercellular communication by grouping cells based on their assigned cluster (17). The communication probabilities are calculated based on the standard mass-action model used in CellChat and subsequently compared interaction networks between Tumor and Normal samples. The differential interaction analysis highlighted those cell-cell pairs which showed enhanced signaling interactions in Tumor compared to Normal (permutation P value <0.05). We concentrated on interaction involving Fibroblasts and T-cells. NicheNet was also applied to support these findings and discover relevant ligand/receptor pairs (18). NicheNet integrates the sender cells' expression of ligands with the receiver cells' expression of receptors and target genes as well as prior knowledge associated with the signaling network. The iCAFs are explored as ligands sources while CD4 Trm are considered as target cells (and vice versa), obtaining a ranked list of ligand activities based on the NicheNet results. Finally, the top ligand-receptor pairs are also validated to determine if they are consistent with the expression patterns observed and whether they showed evidence of spatial co-expression.

Statistical analysis

Cell-type abundance in each patient's tumors was determined by cluster-specific marker genes, in order to conduct survival analysis using the GSVA package (19). Kaplan-Meier curves are generated, and the results are compared with a log-rank test; a P value <0.05 indicated a significant difference. All statistics are calculated with the R statistical programming language.

Results

Single-cell cellular landscape of ccRCC

Using two independent scRNA-seq datasets combined with an external spatial transcriptomics dataset, we established the integrated multi-omics framework for developing robust cellular atlas of ccRCC. The Discovery cohorts of the scRNA-seq comprised GSE210042 (2 normal kidneys and 7 tumors) and GSE156632 (5 normal kidneys and 7 tumors). The visium spatial Transcriptomics data set, GSE175540, was also included to allow for mapping of inferred cell states and interactions back to tissue architecture (*Figure 1A*). After rigorous quality control, normalization, and cross-cohort integration, unsupervised clustering revealed the ccRCC ecosystem consisting of eight major cellular compartments. UMAP embedding demonstrated clearly defined clusters representing ductal cells, T cells, endothelial cells, macrophages, mesangial cells, NK cells, B cells, and mast cells, thus creating a coherent framework from which to perform subsequent high-resolution analysis (*Figure 1B*). To ensure that accurate cell-type annotations are made, we confirmed the lineage identity of each compartment by reference to canonical marker genes for ductal cells (*EPCAM*), T cells (*CD3G*), endothelial cells (*VWF*), macrophages (*CD68*), and mesangial cells (*ACTA2*). Immune subtypes are further supported using NKG7 (NK cells), CD79A (B cells), and TPSAB1 (mast cells) (*Figure 1C*). Collectively, these high-end marker expression patterns support the validity of our comprehensive classification across the integrated dataset.

We further evaluated the tumor-associated reorganization

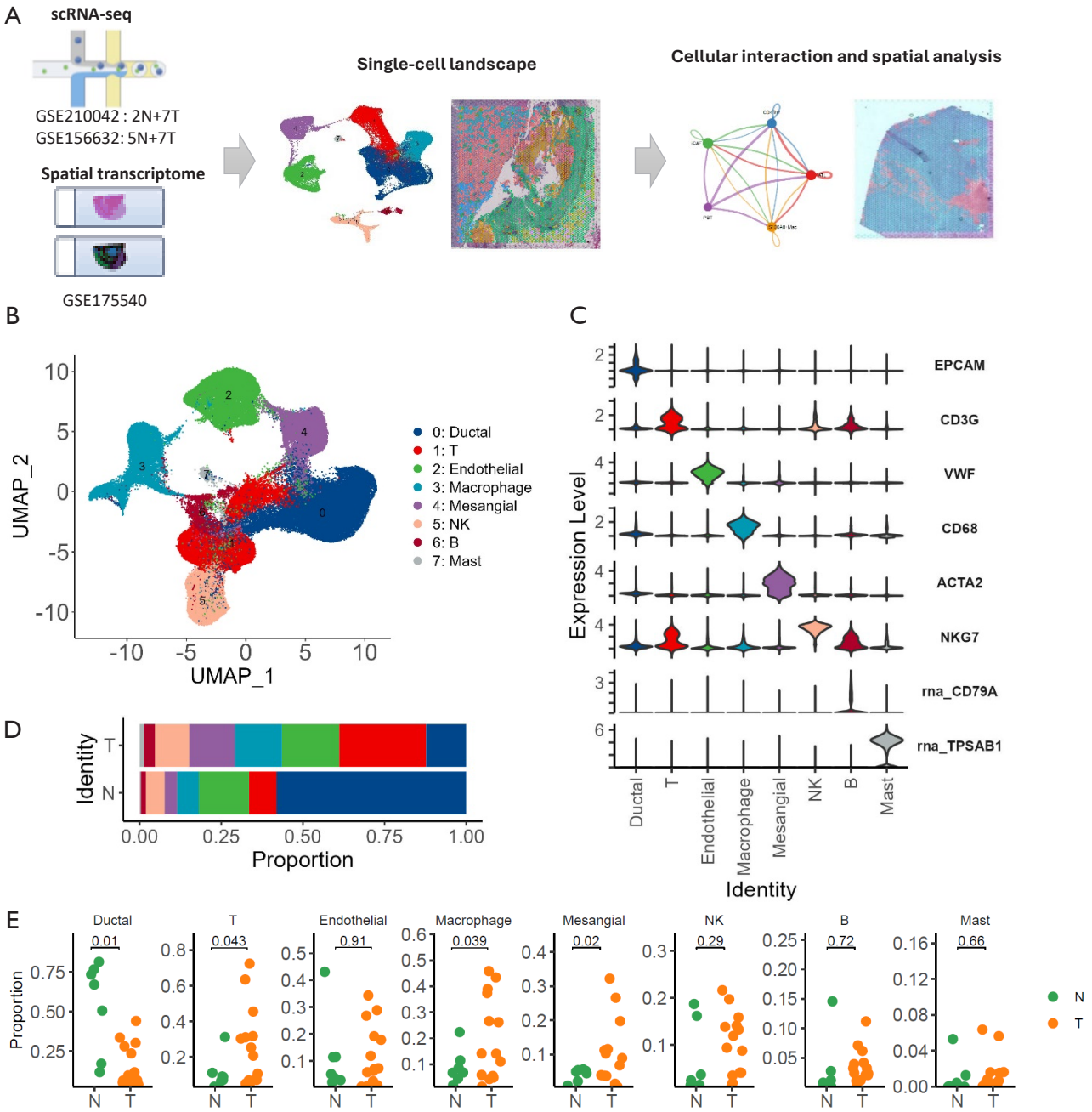

Figure 1 Integrated single-cell and spatial transcriptomics define the cellular landscape of ccRCC. (A) Schematic overview of the study design. Two independent scRNA-seq datasets (GSE210042: 2 normal and 7 tumor samples; GSE156632: 5 normal and 7 tumor samples) are integrated to construct a ccRCC single-cell atlas, followed by validation and spatial mapping using Visium spatial transcriptomics data (GSE175540). (B) UMAP visualization of the integrated scRNA-seq dataset showing eight major cellular compartments, including ductal epithelial cells, T cells, endothelial cells, macrophages, mesangial cells, NK cells, B cells, and mast cells. (C) Dot plot showing canonical marker gene expression used for lineage annotation across major cell types. (D) Stacked bar plots showing the relative abundance of each major cellular compartment in normal kidney (N) and tumor (T) samples. (E) Quantitative comparison of cell-type proportions between N and T samples. Statistical significance was assessed at the sample level; ductal cells, T cells, macrophages, and mesangial cells showed significant tumor-associated shifts. ccRCC, clear-cell renal cell carcinoma; scRNA-seq, single-cell RNA sequencing; UMAP, Uniform Manifold Approximation and Projection.

of cellular constituents within the entire tumor ecosystem by evaluating differences in lineage composition between normal tissues and tumor tissue. The stacked bar graphs showed that the overall proportions differed substantially between the normal tissues and the tumor tissue across the disease progression. Notably, these changes predominately took place within the epithelial, immune, and stromal compartments (*Figure 1D*). These observations are further validated through statistical testing between groups; statistically significant differences are evident for ductal cells (P=0.01), T-cells (P=0.04), macrophages (P=0.04), and mesangial cells (P=0.02). However, endothelial cells (P=0.91), NK-cells (P=0.29), B-cells (P=0.72), and mast cells (P=0.66) did not show any statistically significant shifts within this broad lineage scope (*Figure 1E*). Due to both the significant changes in cellular composition attributed to tumor presence and the established roles of ductal cells, T-cells, macrophages, and mesangial cells in ccRCC development, we prioritized these four cellular compartments for further detailed sub-clustering, functional pathway exploration, and mechanistic conclusions regarding intercellular communication.

An activation-residency-suppression immune triad characterizes the T-cell landscape

To explore the precise characterization of the T-cell adaptive immune compartments in ccRCC, we took advantage of the integrated scRNA-seq atlas of T-cells from ccRCC, producing a detailed map of T-cell diversity. From this map we are able to classify four distinct types of T-cells that can be differentiated functionally and transcriptionally (*Figure 2A*): cytotoxic CD8 T-cells (CytotoxicCD8T), CD8 Resident T-cells (ResidentCD8T), CD4 tissue resident memory T-cells (CD4Trm), and regulatory T-cells (Treg) (*Figure 2A*) which are used for comparisons of compositions, correlations with known T-cell functionality and survival analysis. We validated the biological identity of each of the four T-cell subsets by using markers specific to these populations (*Figure 2B*). The cytotoxic and resident CD8 T-cells are both strongly positive for the CD8A marker. The resident T-cell population expressed the CD69 marker and was associated with tissue residency. The memory-resident phenotype of the CD4Trm-these cells are correlated to their expression levels of the CD4, CD69, and IL7R markers and a more comprehensive signature was displayed in Figure S1A. The Treg cells uniquely expressed the *FOXP3* marker.

We analyzed how these subsets of T-cells redistribute from normal kidneys (N) to tumor samples (T). The proportional bar plots (*Figure 2C*) revealed that over all comparisons, the T-cell landscape was remodeled suggesting that there was a reorganization of T-cell states away from resident and regulatory programs in tumors to effector programs. We calculated per-sample distribution of ResidentC8T, CytotoxicC8T, CD4Trm, and Treg to quantify variability within individual samples and to test for significant inter-sample differences at the group level (*Figure 2D*). ResidentC8T had the greatest difference in T *vs.* N, while CytotoxicC8T did not reach statistical significance yet, CD4Trm nor Tregs are different between groups at this resolution of the analysis. To determine the clustering of genes that defined the different transcriptional programs for each T-cell state subset (*Figure 2E,2F*), we identified differentially expressed cluster specific genes. In addition to the clusters specific to ResidentC8T, CytotoxicC8T was specifically associated with pathways associated with cytolytic activity and inflammatory activation, which agrees with the classical effector T-cell phenotype responsible for direct tumor cell destruction (cytolytic activity). However, ResidentC8T preferentially enriched pathways to produce TNF superfamily cytokines, as well as pathways for the repair of tissue damage and chemotaxis. This indicates that ResidentC8Ts sustain an ongoing local stimulation state in association with tissue residency in response to inflammatory signals and repair responses as opposed to short-term cytolytic activity. Therefore, ResidentC8Ts are in a state of chronic activation but functionally passive and functionally altered. Tregs have primarily been shown to utilize pathways for the regulation of the immune system and the regulation of interleukin12 (IL-12) and interleukin10 (IL-10) pathway signaling, which illustrates the suppressive effects of Tregs on effector immune responses and the establishment of an immunosuppressive microenvironment. Together, these three pathways represent the concept of a ccRCC 'activation-residency-suppression' triad, or the concept of immune exclusion combined with tissue residency and immunoregulation. Moreover, we evaluated the clinical relevance of T cell subsets in ccRCC with respect to patient survival (*Figure 2G*). We found that a higher abundance of Resident CD8T cells was significantly associated with poorer patient survival (log-rank P=0.01), whilst CD4 Trm abundance was inversely related to patient survival (log-rank P=0.05) indicating that tissue resident CD8T cells are associated with adverse clinical outcomes and the presence of dysfunctional (chronically stimulated) immuno-

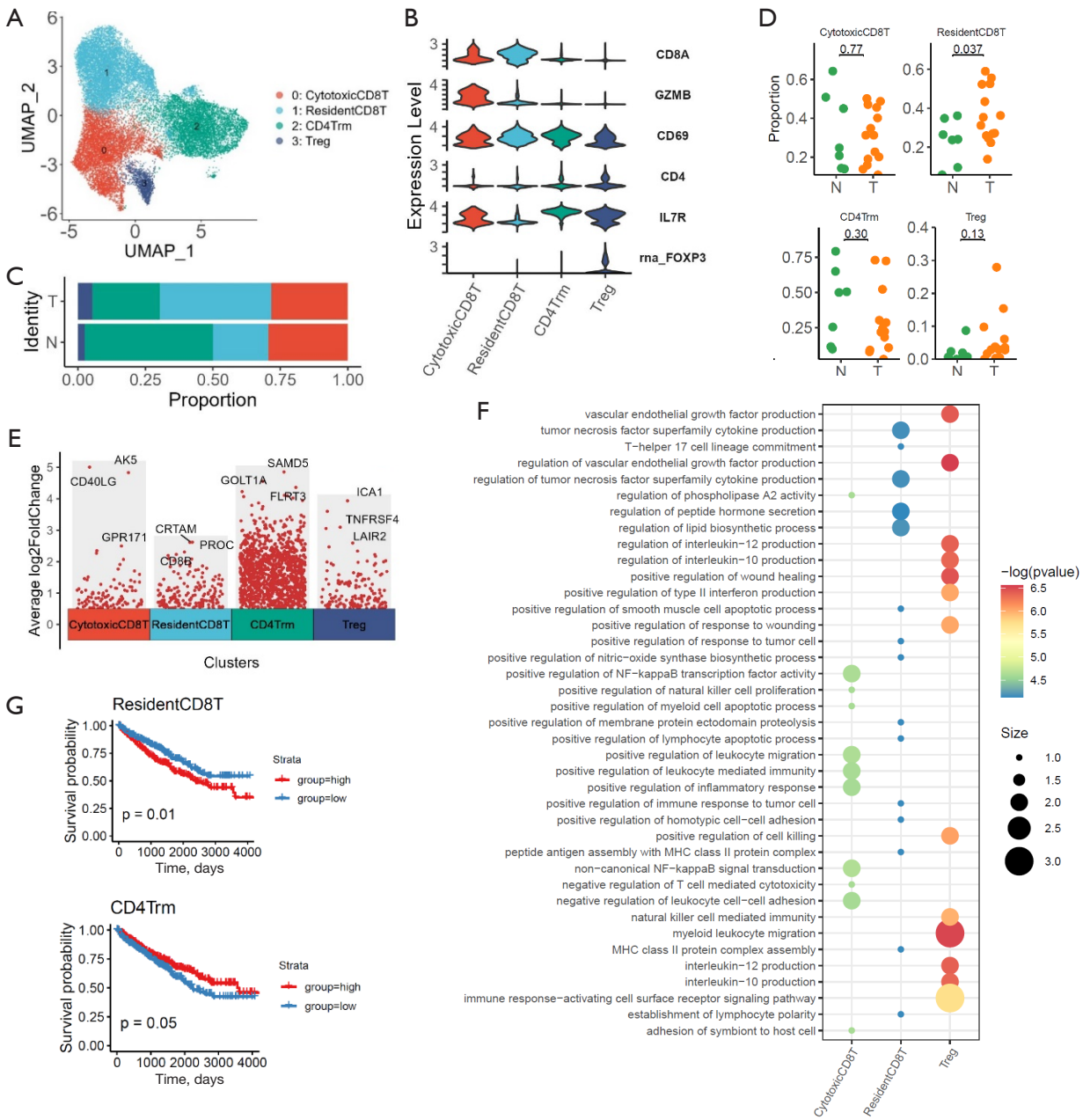

Figure 2 T-cell heterogeneity reveals an activation-residency-suppression immune triad in ccRCC. (A) UMAP visualization of re-clustered T cells, identifying four major T-cell states: CytotoxicCD8T, ResidentCD8T, CD4Trm, and Treg. (B) Feature and dot plots showing expression of representative marker genes used to annotate T-cell subsets, including *CD8A*, *GZMB*, *CD69*, *CD4*, *IL7R*, and *FOXP3*. (C) Stacked bar plots showing the relative abundance of T-cell subsets in normal and tumor samples. (D) Per-sample scatter plots depicting inter-sample variability in T-cell subset proportions; statistical testing identified a significant tumor-associated change in ResidentCD8T abundance. (E) Stacked volcano of cluster-specific differentially expressed genes defining each T-cell subset. (F) Functional enrichment analysis of subset-specific genes, highlighting cytolytic and inflammatory programs in CytotoxicCD8T, chronic inflammatory and tissue-repair-associated programs in ResidentCD8T, and immune regulatory pathways in Treg. (G) Kaplan-Meier survival analysis showing opposite prognostic associations of tissue-resident T-cell subsets, with ResidentCD8T associated with worse survival and CD4Trm associated with improved survival. ccRCC, clear-cell renal cell carcinoma; CD4Trm, CD4 tissue-resident memory T cells; CytotoxicCD8T, Cytotoxic CD8 T cells; ResidentCD8T, resident CD8 T cells; Treg, regulatory T cells; UMAP, Uniform Manifold Approximation and Projection.

suppressive milieu, whereas tissue resident CD4 Trm cells are aligned with favourable immune context.

High-resolution profiling resolves diverse macrophage states

We identified and analyzed the macrophage compartment in ccRCC in detail. To do this, we used the macrophage lineage to generate separate clusters from the integrated atlas and provide dedicated annotations for these clusters (*Figure 3A*). We consistently identified three macrophage states that are present across all the ccRCC samples we analyzed: FOLR2$^+$ macrophages (FOLR2$^+$Mac), S100A8$^+$ macrophages (S100A8$^+$Mac), and a DC (CLEC10A) cluster (*Figure 3B*). After validating our cluster assignments based on marker expression, each of these three clusters was confirmed to represent its own unique transcriptional identity. FOLR2$^+$Mac is characterized as having a tissue-supportive macrophage program, S100A8$^+$Mac represents an inflammatory macrophage state, and DCs have an antigen presentation-related profile characteristic of professional antigen-presenting cells.

We also examined how macrophage populations are distributed across normal kidney (N) and tumor (T) samples. Stacked proportion plots of normal kidney versus tumor samples indicate that remodeling of the macrophage population occurs across normal kidney and tumor samples (*Figure 3C*). Thus, we conclude that ccRCC is characterized by a shift in the balance of tissue-supportive and inflammatory macrophage programs. Finally, to visually depict the IHG observed between ccRCC samples, we plotted sample proportion for each sample (*Figure 3D*) and found that while there was a significant degree of variability between patients with ccRCC in terms of how many macrophages/DCs are present, there was no one predominant direction of shift in macrophage or DC populations across all tumors.

Using cluster-specific differentially expressed genes (*Figure 3E*) and functional enrichment analysis (*Figure 3F*) to characterize the transcriptional programs associated with myeloid subset(s), we determined that FOLR2$^+$Mac signatures are enriched for pathways associated with interleukin-1 regulation, moderate activation of inflammatory programs, and maintenance of tissues, indicating a macrophage phenotype that supports homeostasis while orchestrating immunologic response in a controlled manner. On the other hand, the S100A8$^+$Mac signatures are enriched for immune response and chemotactic pathways, implying a macrophage program that has a greater emphasis on inflammation/recruitment. Lastly, it was found that the predominant functional signatures for DCs are associated with antigen presentation and adaptive immune activation, suggesting that these cells play a role in either priming or sustaining the T-cell response to TME. Despite the clear functional distinctiveness from the profiles described above, Survival analyses did not show any significant association between abundance of any specific myeloid subset (FOLR2$^+$Mac, S100A8$^+$Mac, or DC) and patient outcome. As a whole, our data indicate that while the distinct biological classes of macrophages arising from ccRCC can be classified into three primary functional categories encompassing tissue-supportive macrophages (FOLR2$^+$Mac), inflammatory macrophages (S100A8$^+$Mac), as well as DC (antigen-presenting), their prognostic relevance may be situationally dependent and determined by their spatial localization in addition to interactions with other compartments, such as T cells and stromal niches, rather than orthogonal totals count.

Distinct mesenchymal programs define functional and prognostic diversity

To identify the distinct stromal cellular populations characteristic in ccRCC, we reconsolidated the mesenchymal population using scRNA-seq and created functional annotations for the primary stromal types, as shown in *Figure 4A*. The resulting annotations allowed for the identification of four major transcriptional groups of mesenchymal populations: PDGFRB$^+$ mesenchymal cells (PDGFRB$^+$MC), inflammatory CAFs (iCAFs), myofibroblastic CAFs (myCAFs), and smooth muscle cells (SMCs). With these annotations in hand, we are able to perform a systematic comparison of these populations by their relative abundance of functional programming and relevance to clinical care. Support for this work included the validation of the created annotations using a markers validation strategy as shown in *Figure 4B*. The PDGFRB$^+$MC population exhibited perivascular and renal interstitial-like identities, maintaining mesenchymal properties; the iCAFs displayed an inflammatory myofibroblast phenotype with ECM-associated production, the correlated marker was showed in Figure S1B; the myCAFs expressed a contractile and ECM remodeling phenotype; and the SMC population displayed classical smooth muscle characteristics with vessel-associated gene expression. We characterized remodeling-associated functional state alterations of the four types of fibroblasts as a consequence of the influence of the tumor on these fibroblasts. Comparisons of normal kidney (N) tissue versus tumor (T) tissue using proportional bar graphs illustrating

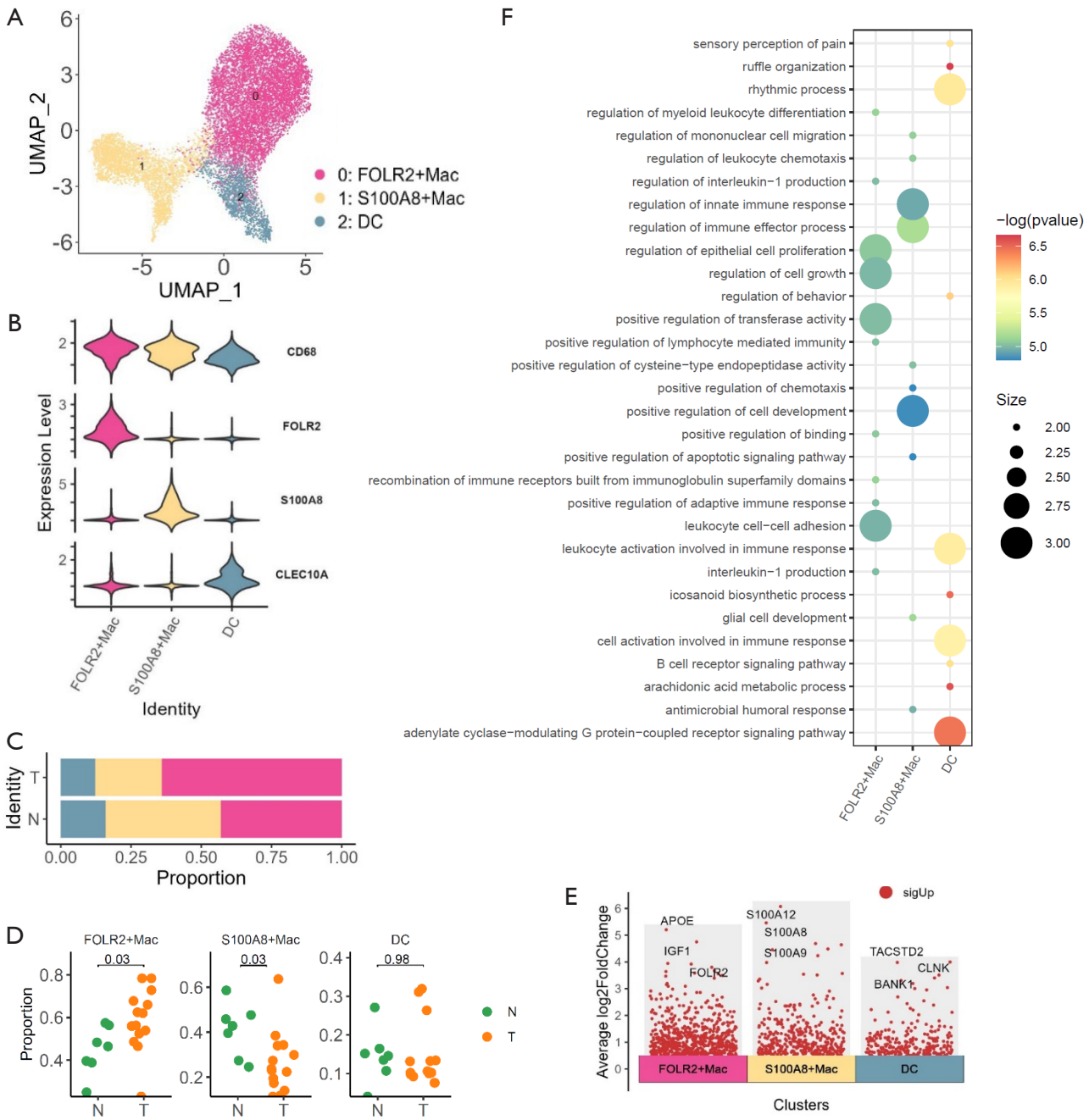

Figure 3 Macrophage heterogeneity defines functionally distinct myeloid states without dominant prognostic impact. (A) UMAP visualization of re-clustered myeloid cells, identifying FOLR2⁺Mac, S100A8⁺Mac, and CLEC10A⁺ DCs. (B) Marker gene expression validating macrophage and DC annotations. (C) Stacked bar plots showing the distribution of myeloid subsets across normal and tumor samples. (D) Per-sample scatter plots illustrating inter-patient variability in myeloid composition. (E) Stacked volcano of differentially expressed genes characterizing each myeloid subset. (F) Gene Ontology and pathway enrichment analysis revealing tissue-supportive and regulated inflammatory programs in FOLR2⁺ macrophages, inflammatory and chemotactic programs in S100A8⁺ macrophages, and antigen presentation pathways in DCs. Survival analyses showed no significant association between individual myeloid subsets and patient outcome. DCs, dendritic cells; FOLR2⁺Mac, FOLR2-positive macrophage; S100A8⁺Mac, S100A8⁺ macrophages; UMAP, Uniform Manifold Approximation and Projection.

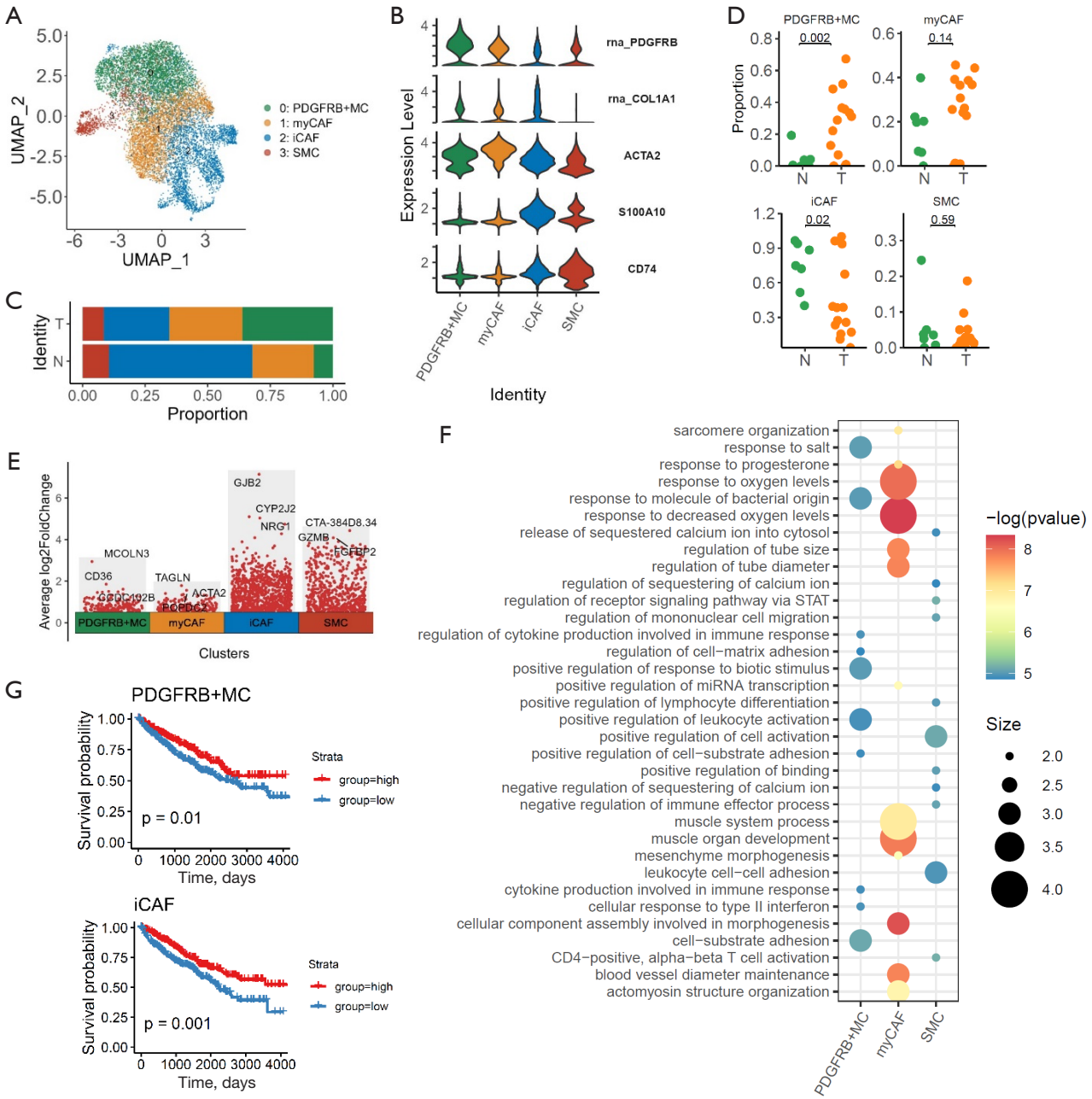

Figure 4 Mesenchymal heterogeneity identifies prognostically favorable PDGFRB⁺MCs and iCAFs. (A) UMAP visualization of mesenchymal cells identifying four stromal populations: PDGFRB⁺MC, iCAFs, myCAFs, and SMCs. (B) Marker-based validation of stromal annotations. (C) Stacked bar plots showing stromal composition in normal and tumor samples. (D) Per-sample scatter plots illustrating stromal heterogeneity across patients. (E) Stacked volcano of stromal subset-specific gene expression. (F) Pathway enrichment analysis showing normal-like interstitial and immune-modulatory programs in PDGFRB⁺MC, inflammatory and ECM-associated programs in iCAFs, and hypoxia- and contractility-related programs in myCAFs. (G) Kaplan-Meier survival analysis demonstrating favorable prognosis associated with higher abundance of PDGFRB⁺MC and iCAFs. CAFs, cancer-associated fibroblasts; ECM, extracellular matrix; iCAFs, inflammatory CAFs; myCAFs, myofibroblastic CAFs; PDGFRB⁺MC, PDGFRB⁺ mesenchymal cells; SMCs, smooth muscle cells; UMAP, Uniform Manifold Approximation and Projection.

relative abundance of mesenchymal populations' abundance in both tissue types (*Figure 4C*) and significant variation among samples within the same condition (*Figure 4D*) demonstrated the existence of large differences between tissue types and confirmed the previously published heterogeneity of ccRCC and its association with stromal cell type variations.

Differential gene expressions have been assessed in prior paragraphs by both assessing differential gene expressions across populations and by assessing the pathways found to be enriched amongst those genes (*Figure 4E*,*4F*). The following pathways are found to be significantly enriched within the population identified as PDGFRB$^+$MC, which are representative of pathways related to stress response, nephron structural development, and moderate alteration in immune status. This suggests that PDGFRB$^+$MC may possess some characteristics or functions of a normal renal interstitial site. Based on the findings of the current study, we conclude that PDGFRB$^+$MC represents a niche of stromal protection for ccRCC and is an area of preserved structural integrity versus fibrotic or heavily altered stroma. The similarity of PAH and cytokeratin signature to functional identities of myCAF and SMC populations indicates that myCAF function in ccRCC relates most closely to the interplay between hypoxia and local vascular systems and that SMC function is implicated more closely with immune system alterations or perivascular immune tone than to the production of ECM as the predominant function of fibroblasts. The present study also assessed the prognostic relevance of the three stromal populations on overall survival (OS) using Kaplan-Meier curves. Importantly, higher levels of PDGFRB$^+$MC are shown to correlate with improved OS outcomes in ccRCC patients and greater levels of iCAF also correlated with improved outcomes (*Figure 4G*). These data suggest that not all factors affecting stromal remodeling in ccRCC are detrimental but rather that some subpopulations of mesenchymal-derived fibroblasts are associated with improved clinical outcomes in ccRCC, especially the preserved PDGFRB$^+$MC niche and the presence of iCAF-producing fibroblasts have the capacity to provide immune support. These data highlight the need for additional studies regarding how to better characterize and understand the spatial and mechanistic interactions of these fibroblast populations through additional studies.

Distinct nephron-derived epithelial states with opposing clinical relevance

This study focused on the epithelial component of ccRCC due to its alteration and importance in how the immune system interacts with the stroma, thus we thoroughly examined epithelial cells (the ductal tubular component). After re-cluster the data, two epithelial states are identified in the ductal compartment: proximal straight tubule (PST) and ascending thin limb cells (ATL), both of which share nephron-derived program similarities within the ccRCC microenvironment (*Figure 5A*). Validation of the two epithelial states is represented in *Figure 5B*. Both epithelial states have lineage-specific transcriptional characteristics, including those associated with nephron segments; this demonstrates that they represent the divergence of PST and ATL functional similarities and differentiate the two states for comparison of both clinical and functional features. We analyzed the proportion of PST and ATL found in normal kidney and tumor sample tissues and plotted the results on a proportion plot (*Figure 5C*) that demonstrated how the proportions change with the respective conditions. From scatter plots of individual patient samples (*Figure 5D*), it is evident there is a large amount of inter-sample variability, indicating that epithelium composition differs among tumors (and possibly) will depend on local mechanisms (e.g., degree of differentiation, as well as differing influences from the local microenvironment), and will change rapidly as ccRCC disease progresses. Next, we identified the respective transcriptional programs most associated with PST and ATL by identifying differentially expressed genes (*Figure 5E*) and enrichment analysis on PST and ATL signature genes (*Figure 5F*) was performed. The authors observed that most PST-derived signature genes are enriched for metabolic pathways associated with amino acid/nucleotide metabolism and transmembrane transport functions typical of normal proximal tubules, demonstrating the PST state reflects a more stable, structurally well-preserved nephron component. In contrast, the majority of ATL-derived signature genes are associated with immune response, epithelial-matrix adhesion, and innate immune sensing mediated by toll-like receptor (TLR) signaling pathways, indicating that the ATL state may represent an epithelium that is actively involved in responding to inflammation, as well as reorganizing the interface between the epithelium and stroma of the ccRCC TME. Finally, the authors evaluated the clinical significance of the two states in the context of survival analysis (*Figure 5G*) and identified that high abundance of ATL was associated with poorer survival rates, while high abundance of PST was associated with improved survival rates, demonstrating the divergent prognostic implication of these two epithelial

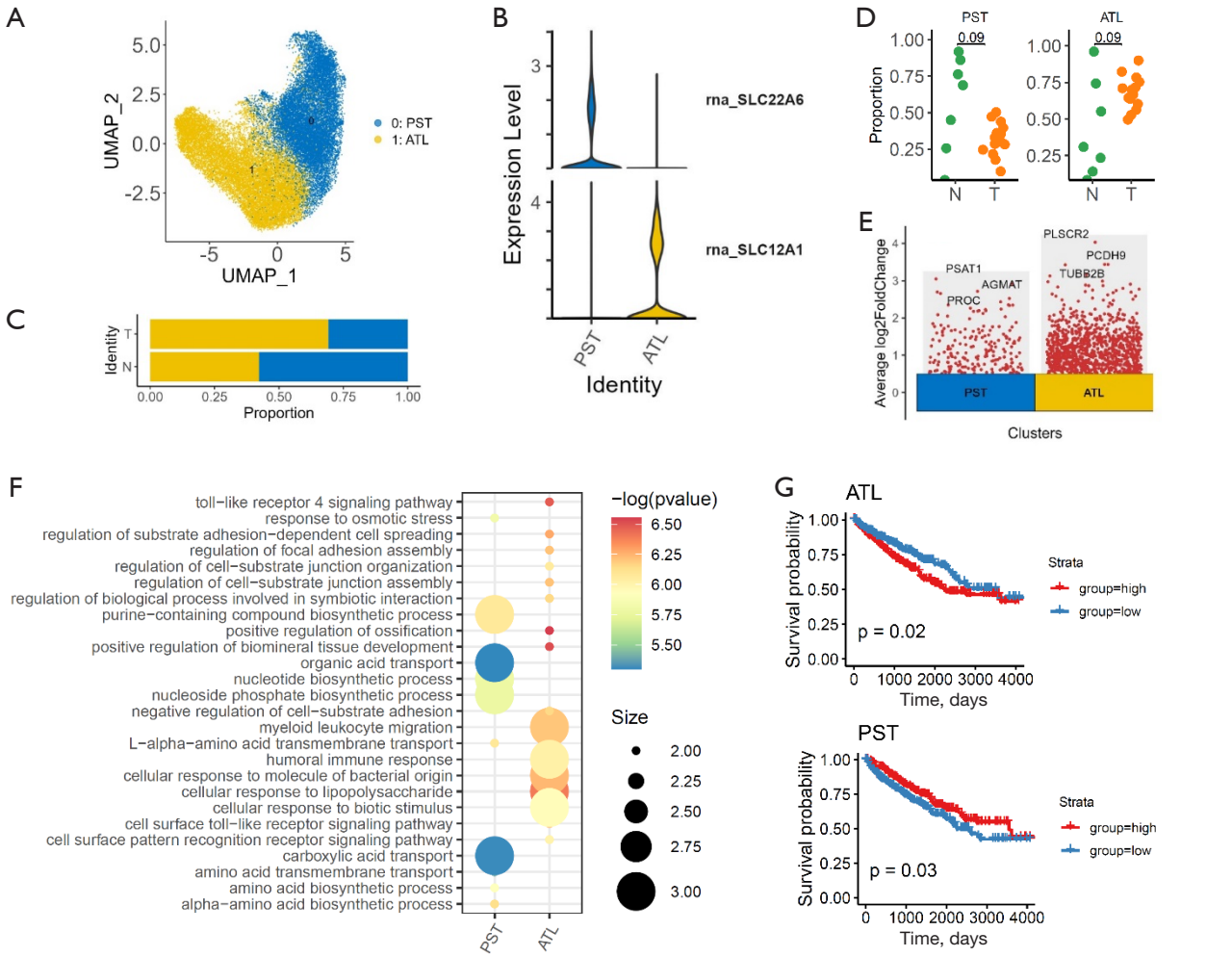

Figure 5 Ductal epithelial heterogeneity delineates prognostically divergent PST and ATL programs. (A) UMAP visualization of re-clustered ductal epithelial cells identifying PST and ATL cells. (B) Expression of lineage-specific markers validating PST and ATL identities. (C) Relative abundance of PST and ATL across normal and tumor samples. (D) Per-sample scatter plots showing inter-tumoral variability in epithelial composition. (E) Differentially expressed genes defining PST and ATL programs. (F) Functional enrichment analysis revealing metabolic and transport pathways in PST and immune sensing, adhesion remodeling, and Toll-like receptor signaling in ATL. (G) Kaplan-Meier survival analysis showing worse prognosis associated with ATL enrichment and improved survival associated with PST abundance. ATL, ascending thin limb; PST, proximal straight tubules; UMAP, Uniform Manifold Approximation and Projection.

program similarities. In conclusion, the data from this study suggest that the two distinct epithelial states of ccRCC are derived from two separate transcriptional programs, as the nature of the PST *vs.* ATL states differ based on their biological properties, with PST state being more stable and, thus, representing a relatively favorable less inflammatory tissue environment, while the ATL state reflects increased inflammation, likely stress of the epithelium, and maladaptive epithelial-stromal interaction leading to advanced disease progression in ccRCC.

Spatially resolved analysis identifies an iCAF-CD4Trm immune-supportive niche

The aim of this analysis was to gain insight into how a healthy stromal profile relates to the protection of T-cell phenotypes at the tissue level in ccRCC patients. To achieve this goal, we carried out a cellular communication network analysis using the CellChat platform to compare intercellular communication networks in primary tumor *vs.* normal samples on differential cell populations identified

through Single-Cell RNA-Seq data from ccRCC patient tissue samples. Using intercellular signal events identified by Single-Cell RNA-Seq analyses, the cells that demonstrated the most significant increase in predicted intercellular signaling events between tumor and normal sample tissues are iCAF-CD4Trm and Resident CD8T-PDGFRB$^+$ mesenchymal cells (*Figure 6A*). Both cell types showed significant differences in their predicted intercellular signals, but only the iCAF-CD4Trm interaction was confirmable at the tissue level using spatial transcriptomics and Single-Cell RNA-Seq data. The absence of spatial concordance for the Resident CD8T-PDGFRB$^+$ mesenchymal cell interaction suggests that the iCAF-CD4Trm interaction is more critical in the ccRCC TME; therefore, we focused on investigating this pathway further. To identify the iCAF-CD4Trm microenvironment *in situ*, we defined "mixed spots" in the Spatial Transcriptomics dataset where both iCAF phenotype and CD4Trm phenotype are found to be enriched (*Figure 6B*). The spatial distribution analysis of these mixed spots demonstrated that they are preferentially localized to the Tumor-Stroma Interface, rather than dispersing evenly throughout the entire tissue section, implying that an Immune-Stromal niche in ccRCC has a specific spatial configuration. The results of the co-localization analyses corroborated the iCAF/CD4Trm mixed spot findings and confirmed that CD4Trm niches are concentrated in iCAF high regions; therefore, there is biological evidence that the previous conclusions drawn from Single-Cell RNA-Seq analyses are valid (*Figure 6C*). Next, we described the iCAF-CD4Trm immune-stromal niche's proposed mechanism of interaction by integrating the predicted intercellular communication pathways through the CellChat analyses; therefore, these results also give mechanistic insight into the formation and establishment of a protective immune-supportive environment surrounding CD4Trm cells through the establishment of an ECM (*Figure 6D*). In order to determine which ligand-receptor interactions drive these interactions, we applied NicheNet to predict potential ligand-receptor interactions using iCAF and CD4Trm cells as sources. Our results indicated that the predominant interface predicted by NicheNet was a ligand-receptor interaction resulting from ECM anchoring proteins (*Figure 6E*). Among the ligands predicted for iCAFs, fibronectin (FN1) was identified as a top potential ligand for CD4Trm cells predicted to bind via integrin receptors on CD4Trm cells. FN1 has been shown to bind to CD4Trm cells via the integrin receptors ITGA5/ITGB1, thus demonstrating a high potential for interaction. Collectively, the results of all of our integrative analyses support a model by which iCAFs develop and sustain an immune-supportive microenvironment by forming an ECM-based anchoring system that stabilizes the location and function of CD4Trm cells via adhesion-dependent retention of CD4Trm cells and support of CD4Trm cells from the ECM. Overall, we feel that this information provides a spatial context and mechanistic rationale for the presence of iCAF-CD4Trm "mixed spots" observed in ccRCC patients.

Discussion

In the present investigation, single-cell and spatial transcriptomics have allowed us to assess the complete immune and stromal environment of ccRCC. We found a unifying theme across our findings: the spatially organized TME has been demonstrated to contain tumor niches that may be supportive of anti-tumor immune responses or may promote immunosuppression, and that organization is associated with CAF subsets. As such, our discovery of a CAF-T cell niche, represented by the presence of iCAFs and CD4$^+$TRM T cells, supports immune surveillance and correlates with improved survival; thus, highlighting an underappreciated pro-immunogenic role for a specific subset of CAFs in ccRCC, fundamentally conflicting with the long-held notion regarding the uniform immunosuppressive actions of CAFs. Our findings can be aligned with emergent information regarding the functional heterogeneity of CAFs, which can promote or inhibit immune responses in the TME. Prior to our findings, CAFs in ccRCC (and other cancers) are considered to be involved with the immune evasion of tumors via dense ECM production that inhibits T cell migration to tumor sites, release immunosuppressive cytokines (IL-6, TGF-β) and recruit Treg and myeloid suppressive cells (20). The ccRCC has also been shown to use many of the previously established mechanisms of immunosuppression through stromal-mediated pathways in addition to others that have been previously characterized in ccRCC. Among these pathways are the CD27-CD70 signaling pathway and the HLA-G/ILT inhibitory pathway (21-23). CD70 overexpression on tumor cells can lead to chronic stimulation of CD27 resulting in dysfunction of T-cells. HLA-G interactions with ILT family of receptors can in turn suppress effector immune cell responses. While we did not detect a dominant or spatially enriched transcriptional program of CD27-CD70 or HLA-G/ILT in our data reanalysis of the single cell and spatial dataset. Based on this, we do not dispute previous reports of these

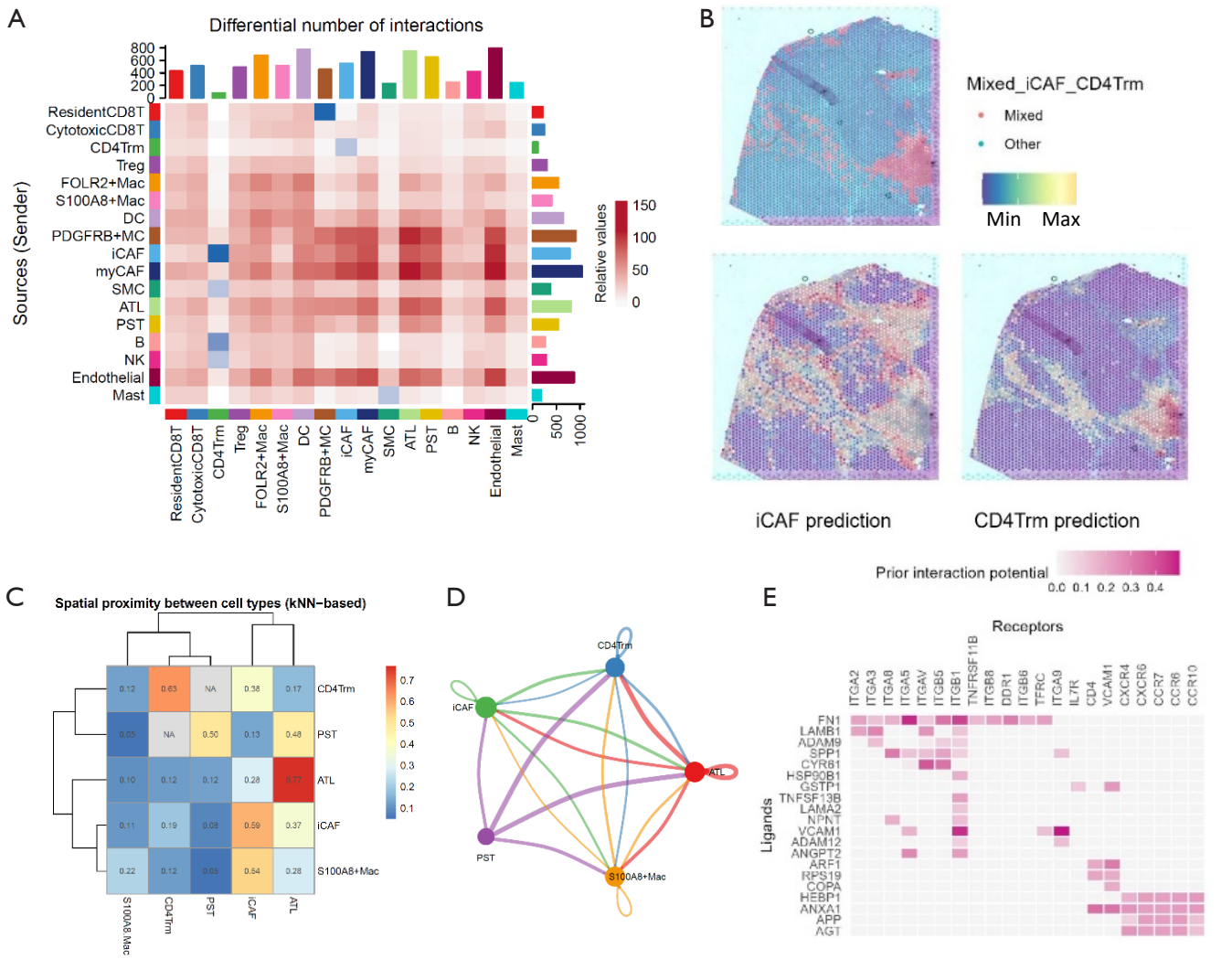

Figure 6 Spatial validation identifies an iCAF-CD4Trm immune-supportive niche in ccRCC. (A) Differential CellChat analysis showing tumor-associated gains in predicted cell-cell communication, highlighting iCAF-CD4Trm and ResidentCD8T-PDGFRB^{+}MC interactions. (B) Spatial transcriptomic mapping of iCAF-CD4Trm mixed spots, defined by concurrent enrichment of iCAF and CD4Trm signatures, showing preferential localization at tumor-stroma interfaces. (C) Spatial co-localization analysis confirming overlap between iCAF-high and CD4Trm-enriched regions. (D) Pathway-level CellChat analysis illustrating dominant outgoing signaling from iCAFs toward CD4Trm in tumor tissues. (E) NicheNet analysis prioritizing extracellular matrix-integrin signaling, with FN1-ITGA5/ITGB1 identified as the top-ranked ligand-receptor axis mediating iCAF-CD4Trm interaction. ccRCC, clear-cell renal cell carcinoma; FN1, fibronectin; iCAF-CD4Trm, inflammatory cancer-associated fibroblast-CD4 tissue resident memory T-cells; PDGFRB^{+}MC, PDGFRB^{+} mesenchymal cells; ResidentCD8T, resident CD8 T cells.

mechanisms but suggest that they may still exist as stimulus specific or context dependent pathways, however, these are not prominently observed in our cohort. Additionally, it is also possible that post-transcriptional regulation, levels of protein expression or tumor evolutionary stage could potentially affect the functional implications of these pathways in the context of what we observed through transcriptomic profiling. Presently, our myCAF population of αSMA high TGF-β-responsive fibroblasts supported the immune exclusion and angiogenesis characteristic of tumors and therefore aligns with previous studies. Importantly, we observed high numbers of CAFs, especially

when present alongside limited CD8 T cell infiltration, to correlate with poor outcomes in immunotherapy; however, our identification of the iCAF-CD4 Trm T cell niche provides a more complex view. Inflammatory CAFs, commonly associated with tumor-promoting inflammatory responses, can support the retention of T helper cells via a physical anchoring scaffold (FN1). This has also been observed in several studies examining other malignancies, including the report by Kerdidani *et al.* that the MHC II+ CAF population stimulated $CD4^+$ T cell proliferation and are able to suppress tumor growth via mechanisms identified in the study (7). Several recent pan-cancer analyses using spatial evaluation methods have discovered myCAF populations collaborating with immune cells; for example, antigen presenting CAFs have been discovered in both pancreatic cancer and melanoma, and could present antigens to $CD4^+$ T cells, although they are frequently deficient in co-stimulatory properties (24). Our investigations revealed that while iCAFs do not appear to express high levels of MHC II gene products, they will likely not directly present tumor-specific antigens to $CD4^+$ T cells. It is more likely that their support to $CD4^+$ T cells occurs in a structural and paracrine manner, providing T cell survival factors, such as FN1 or IL-1 and possibly IL-6, but likely within a homeostatic environment and less so under inflammatory conditions. It is also interesting to note that we found evidence that IL-6 expression occurs in iCAFs along with FN1, as IL-6 promotes proliferation of T cells and is often thought to be immunosuppressive in chronic inflammatory settings. However, it is also possible that IL-6 signaling may aid in developing TRM cells (via the STAT3 pathway). Overall, in our ccRCC data, iCAF-derived factor seems to play essential roles in supporting the continued presence of $CD4^+$ T cell pools that have not attained terminal exhaustion.

FN1-integrin α5β1 signaling was recently identified as a critical modulator of the CAF-Trm cellular microenvironment. FN1 is one of the main components of the provisional ECM within tumors and integrin α5β1 (made up of ITGA5 and ITGB1) acts as the primary receptor for FN1 on leukocytes. A significant finding was the identify of high levels of α5 integrin in cancers found on tissue residing T cells which may aid in identifying tumor-infiltrating lymphocytes with tissue retention (25). A recent study using melanoma has also shown that $CD8^+$ Trm cells upregulated VLA-1 (an α1β1 integrin), which binds collagen, as collagen helps to anchor Trm cells to the fibrous stroma (26). Therefore, like the role of FN1 for CD8 Trm cells, the binding of FN1 to integrin α5β1 may have a similar role in CD4 Trm cells in ccRCC. Our findings provide evidence to support this concept: FN1 and ITGA5/ITGB1 are spatially co-localized in the stable niche—FN1 and ITGA5/ITGB1 are found to be spatially co-expressed and correlated in a stable niche. Functionally, binding of α5β1 provides survival signals via FAK and the Src family of kinases and may induce a state of quiescence or "stem cell-like" behavior rather than allow for immediate or acute release of effector cytokines (27). This is consistent with our findings of a lack of high levels of IFN-γ and granzyme B production from CD4 Trm located within the niche—while not exhibiting acute cytotoxicity, they persist in the tissue and theoretically may be able to be reactivated when needed. Thus, by anchoring these T cells, the iCAF niche may create a pool of ready helper T cells to be used in the tumor for coordinating responses from innate immune cells and supporting CD8 T cell responses. Additionally, we observed that tumors with a strong CAF-CD4 Trm niche had an increased infiltration of conventional CD8 T cells, which may indicate that they are operating in a more supportive microenvironment.

The relationship between spatial immune niches and immunotherapy response was evaluated in our study. One recent study of non-small-cell lung cancer (NSCLC) with spatial transcriptomics identified five different immunogenic microenvironments, as well as high CXCL9/CXCL10 chemokine expression associated with positive response to programmed death-1 (PD-1) antibody treatment among patients that had a CD8-T cell/macrophage rich microenvironment (28). It is interesting to speculate that because some patients have CAF-trm niches as pre-existing pockets of $CD8^+$ T cells that could be reinvigorated as a result of immune checkpoint inhibition; these patients may respond better to immunotherapy than patients whose tumors are CAF-rich but Trm-poor. This notion is supported by findings that patients with high stromal gene expression and low T cell expression have poor clinical outcomes from immunotherapy in RCC. Therefore, incorporating a larger dataset to assess both the spatial component and quantity of the stromal-immune interactions will enhance the prognostic and predictive accuracy of ccRCC.

Our analysis provides additional supporting evidence regarding the immune-stroma interaction in solid malignancies. The concept of an "immune-supportive stroma" is becoming more accepted. In colorectal carcinoma, it was demonstrated that a specific subset of fibroblasts may

draw T-cells to that area and was found to correlate with prolonged survival (29); it may actually behave similarly to lymphoid tissue stroma in those solid tumors. Likewise, in breast carcinoma, FAP$^+$ CAFs are usually immunosuppressive, but there is a subset that makes chemokines that attract T-cells into tertiary lymphoid structures and that correlate with increased immune activity (30). Therefore, the balance of the pro- and anti-immune characteristics of the fibroblasts may determine if the tumor is "hot" or "cold". ccRCC has traditionally been thought of as an immunogenic tumor, however, paradoxically, it has a relatively high degree of immune infiltration yet many of those immune cells in the TME are ineffective. Our data showed that ccRCC has a distinct spatial context of immune organization: some areas with "tissue-resident, supportive" immunity which if enhanced would likely be able to control the tumor. This supports a model for targeting the remodeling of the CAF or expanding favorable niches to tilt the balance. For example, TGF-β inhibitors may reduce how myCAFs exclude T-cells and have demonstrated some level of effectiveness when used in combination with checkpoint blockade therapies in other solid malignancies (31). Our results suggest that another approach may be to try to improve on the FN1-ITGA5 interaction or downstream signals to enhance your ability to retain Trms. Interestingly, targeting the FN1 itself may work. There are peptides that modulate FN1-integrin signaling as a method for normalizing the tumor vasculature and the tumor's immune response. It is also possible that completely inhibiting FN1 could be counterproductive as that could disrupt the beneficial niche between the CAFs and Trms. A better approach could be to encourage the development of lymphoid-like stroma niches.

There are several caveats to this work. First, while our study looks at multiple patients, the total number of patients included is relatively small so further validation will be required using larger, independent cohorts. Second, with a spatial transcriptomic resolution of approximately 50 µm/spot, it is difficult to know exactly what type of cells exist within the spot, which is why we inferred co-localization. Spatial technologies capable of providing single-cell resolution would give an understanding of the exact contacts between cells. Third, functional validation of the FN1-α5β1 mechanism has not been completed in this study, and our conclusions regarding iCAF influence on Trm survival are based on both correlative data and existing literature. Experimental verification that iCAFs prolong the survival of Trm, or that the disruption of FN1-α5β1 contacts within co-cultures decreases Trm maintenance, is necessary. These findings provide insights regarding the potential application of our study's results in therapeutic interventions. Specifically, the results of this study illustrate that ccRCC prognosis is driven by specific states of cells and their location with respect to one another rather than by the total number of cells making up the immune and stromal component of the tumor. A composite signature of the integration of CD4 Trm, iCAF, PDGFRB$^+$ mesenchymal, and PST-like epithelial programs may facilitate a higher quality of risk stratification through mechanisms that differ from those of currently used stratifies. In addition, when developing therapeutic strategies targeting the immune system, it is important to consider re-programming the interaction of microenvironmental elements, rather than the development of a broad-based cell population targeting therapeutic strategy. Further study is warranted to confirm the causative relationship of FN1-integrin signaling in CD4 Trm retention, as well as to understanding the dynamics associated with the evolution of these niches during the therapeutic process. Similar to the current study, future studies will require the integration of longitudinal evaluation of patient samples with higher resolution spatial technology to facilitate the determination of whether the protective niches described in the current study can be induced or expanded therapeutically.

Conclusions

Our study identifies an immuno-stromal niche in ccRCC defined by iCAFs and CD4 Trm cell types, which allows us to link states and cellular signals through the ECM to better clinical outcomes. Using a combination of scRNA-seq and spatial transcriptomics, we showed that the development of effective anti-tumor immune responses in ccRCC is not simply a function of immune cell abundance but rather influenced by the specific states of those immune cells as well as the spatial relationships of those immune cells within a given niche. These findings provide evidence that the interaction of iCAF and CD4 Trm cell types is mechanistically and spatially responsible for contributing to protective immunity. Overall, these studies provide a framework to develop targetable immune-supportive niches for precision immunotherapy for patients with ccRCC.

Acknowledgments

None.

Footnote

Peer Review File: Available at https://tau.amegroups.com/article/view/10.21037/tau-2026-1-0017/prf

Funding: This work was supported by Zhejiang Provincial Department of Education Research Project (Natural Sciences) (No. Y202353954) to Z.H., National Natural Science Foundation of China (No. 82403511) and Zhejiang Provincial Natural Science Foundation (No. LQ24H160005) to F.W.

Conflicts of Interest: All authors have completed the ICMJE uniform disclosure form (available at https://tau.amegroups.com/article/view/10.21037/tau-2026-1-0017/coif). Z.H. reports receiving support from Zhejiang Provincial Department of Education Research Project (Natural Sciences, No. Y202353954). F.W. reports receiving support from National Natural Science Foundation of China (No. 82403511) and Zhejiang Provincial Natural Science Foundation (No. LQ24H160005). The other author has no conflicts of interest to declare.

Ethical Statement: The authors are accountable for all aspects of the work in ensuring that questions related to the accuracy or integrity of any part of the work are appropriately investigated and resolved. The study was conducted in accordance with the Declaration of Helsinki and its subsequent amendments.

References

1. Burgers FH, van der Mijn JCK, Seijkens TTP, et al. Immunological features of clear-cell renal-cell carcinoma and resistance to immune checkpoint inhibitors. Nat Rev Nephrol 2025;21:687-701.
2. Davidson G, Helleux A, Vano YA, et al. Mesenchymal-like Tumor Cells and Myofibroblastic Cancer-Associated Fibroblasts Are Associated with Progression and Immunotherapy Response of Clear Cell Renal Cell Carcinoma. Cancer Res 2023;83:2952-69.
3. Wang M, Zhao Y, Xu K, et al. Cancer-associated fibroblasts in clear cell renal cell carcinoma: functional heterogeneity, tumor microenvironment crosstalk, and therapeutic opportunities. Front Immunol 2025;16:1617968.
4. Zheng X, Jiang K, Xiao W, et al. CD8(+) T cell/cancer-associated fibroblast ratio stratifies prognostic and predictive responses to immunotherapy across multiple cancer types. Front Immunol 2022;13:974265.
5. Peng YL, Xiong LB, Zhou ZH, et al. Single-cell transcriptomics reveals a low CD8(+) T cell infiltrating state mediated by fibroblasts in recurrent renal cell carcinoma. J Immunother Cancer 2022;10:e004206.
6. Xiao Z, Puré E. The fibroinflammatory response in cancer. Nat Rev Cancer 2025;25:399-425.
7. Kerdidani D, Aerakis E, Verrou KM, et al. Lung tumor MHCII immunity depends on in situ antigen presentation by fibroblasts. J Exp Med 2022;219:e20210815.
8. Seo ES, Lee SK, Son YM. Multifaceted functions of tissue-resident memory T cells in tumorigenesis and cancer immunotherapy. Cancer Immunol Immunother 2025;74:184.
9. Byrne A, Savas P, Sant S, et al. Tissue-resident memory T cells in breast cancer control and immunotherapy responses. Nat Rev Clin Oncol 2020;17:341-8.
10. Anadon CM, Yu X, Hänggi K, et al. Ovarian cancer immunogenicity is governed by a narrow subset of progenitor tissue-resident memory T cells. Cancer Cell 2022;40:545-557.e13.
11. Park SL, Buzzai A, Rautela J, et al. Tissue-resident memory CD8(+) T cells promote melanoma-immune equilibrium in skin. Nature 2019;565:366-71.
12. Pichler R, Siska PJ, Tymoszuk P, et al. A chemokine network of T cell exhaustion and metabolic reprogramming in renal cell carcinoma. Front Immunol 2023;14:1095195.
13. Zhang M, Zhai W, Miao J, et al. Single cell analysis reveals intra-tumour heterogeneity, microenvironment and potential diagnosis markers for clear cell renal cell carcinoma. Clin Transl Med 2022;12:e713.
14. Meylan M, Petitprez F, Becht E, et al. Tertiary lymphoid structures generate and propagate anti-tumor antibody-producing plasma cells in renal cell cancer. Immunity 2022;55:527-541.e5.
15. Satija R, Farrell JA, Gennert D, et al. Spatial reconstruction of single-cell gene expression data. Nat

Biotechnol 2015;33:495-502.
16. Wu T, Hu E, Xu S, et al. clusterProfiler 4.0: A universal enrichment tool for interpreting omics data. Innovation (Camb) 2021;2:100141.
17. Jin S, Guerrero-Juarez CF, Zhang L, et al. Inference and analysis of cell-cell communication using CellChat. Nat Commun 2021;12:1088.
18. Browaeys R, Saelens W, Saeys Y. NicheNet: modeling intercellular communication by linking ligands to target genes. Nat Methods 2020;17:159-62.
19. Hänzelmann S, Castelo R, Guinney J. GSVA: gene set variation analysis for microarray and RNA-seq data. BMC Bioinformatics 2013;14:7.
20. Freeman P, Mielgo A. Cancer-Associated Fibroblast Mediated Inhibition of CD8+ Cytotoxic T Cell Accumulation in Tumours: Mechanisms and Therapeutic Opportunities. Cancers (Basel) 2020;12:2687.
21. Benhamouda N, Sam I, Epaillard N, et al. Plasma CD27, a Surrogate of the Intratumoral CD27-CD70 Interaction, Correlates with Immunotherapy Resistance in Renal Cell Carcinoma. Clin Cancer Res 2022;28:4983-94.
22. Sam I, Ben Hamouda N, Alkatrib M, et al. The CD70-CD27 Axis in Cancer Immunotherapy: Predictive Biomarker and Therapeutic Target. Clin Cancer Res 2025;31:2872-81.
23. Rouas-Freiss N, LeMaoult J, Verine J, et al. Intratumor heterogeneity of immune checkpoints in primary renal cell cancer: Focus on HLA-G/ILT2/ILT4. Oncoimmunology 2017;6:e1342023.
24. Hung J, DuPage M. Association of cancer-associated fibroblast composition with CD4 T cells in pancreatic ductal adenocarcinoma. Cancer Res 2025;85:2572.
25. Chernosky NM, Tamagno I. The Role of the Innate Immune System in Cancer Dormancy and Relapse. Cancers (Basel) 2021;13:5621.
26. Chen X, Zheng Y, Man X, et al. Tissue-resident memory T cells and their function in skin diseases. Chin Med J (Engl) 2025;138:1175-83.
27. Hou J, Yan D, Liu Y, et al. The Roles of Integrin α5β1 in Human Cancer. Onco Targets Ther 2020;13:13329-44.
28. Lin W, Wang Y, Li M, et al. Tumor treating fields enhance anti-PD therapy by improving CCL2/8 and CXCL9/CXCL10 expression through inducing immunogenic cell death in NSCLC models. BMC Cancer 2025;25:489.
29. Wang Y, Chen Z, Zhao G, et al. Cancer-Associated Fibroblast Risk Model for Prediction of Colorectal Carcinoma Prognosis and Therapeutic Responses. Mediators Inflamm 2023;2023:3781091.
30. Bonneau C, Eliès A, Kieffer Y, et al. A subset of activated fibroblasts is associated with distant relapse in early luminal breast cancer. Breast Cancer Res 2020;22:76.
31. Milosevic V, Östman A. Interactions between cancer-associated fibroblasts and T-cells: functional crosstalk with targeting and biomarker potential. Ups J Med Sci 2024. doi: 10.48101/ujms.v129.10710.

Cite this article as: Hu Z, Wang F, Lin Y. Spatial multi-omics reveals a cancer-associated fibroblast-T cell niche sustaining tissue-resident immunity in clear-cell renal cell carcinoma. Transl Androl Urol 2026;15(4):108. doi: 10.21037/tau-2026-1-0017